

## EXPERIMENTAL STUDY OF HIGH LIQUID VISCOSITY OIL-GAS FLOWS USING ECT AND GAMMA RADIATION METHODS

Archibong Archibong-Eso<sup>1,2</sup>, Yahaya D. Baba<sup>1,3\*</sup>, Aliyu Aliyu<sup>1,4</sup>, Nonso Okeke<sup>1</sup>, Abdulwahab Giwa<sup>3</sup>

<sup>1</sup> Oil & Gas Engineering Centre, Cranfield University, UK

<sup>2</sup> Cross River University of Technology, Calabar, Nigeria

<sup>3</sup> Department of Chemical and Petroleum Engineering, Afe Babalola University, Ado-Ekiti, Nigeria

<sup>4</sup> School of Mechanical Engineering, Pusan National University, 609-735, Busan, Republic of Korea

Received October 19, 2017; Accepted January 8, 2018

---

### Abstract

Electrical capacitance tomography (ECT) and gamma ray densitometry have found applications in multiphase flows as both have been used to visualize flow patterns in the process, nuclear, chemical and oil-gas industries. However, liquid viscosity is often limited to about 10 cP in most of these applications. This study evaluates the suitability of ECT in the monitoring of multiphase flow consisting of heavy-oil (up to 7500 cP) and gas. Heavy-oil is of interest because of its huge reserves, increasing world energy demand, dwindling conventional-oil reserves, etc. The results obtained showed that ECT performed well in flow visualization and measurement of high-viscous oil/gas flows. Flow patterns identified included plug, slug, pseudo-slug (blow-through-slug) and annular flows. Liquid holdup measurements were found to be within  $\pm 10\%$  and  $\pm 5\%$  error in the static stratified and static annular test, respectively, based on the LBP algorithm while in dynamic test, it was considerably dependent on flow patterns and the LBP. Comparatively, high definition video recordings, pictures and gamma rays densitometer were used to validate the flow patterns identified by ECT.

**Keywords:** High viscosity oil; flow patterns; gamma rays; multiphase flow; liquid holdup.

---

## 1. Introduction

The foray of tomography into chemical and process industries is hinged on its several successes in medical applications. Multiphase flows exist widely in process and chemical industries such as nuclear, food, agro-allied, oil and gas, water, polymer, textile, etc. Prior knowledge of the behaviour of the phase distribution plays a significant role in process control, process equipment design, pumps and pumping systems design, quality control, safety assurance, process flow assurance, etc. The complex nature of multiphase flow, which is characterised by deformable phase interface, phase inversion, phase slip, as well as the variations of the phase distribution and the velocity profiles with temporal and spatial coordinates, makes it very difficult to measure its phase quantity and distribution (flow pattern or flow regime). Tomography thus becomes important as it can be utilized as a valuable tool in flow visualization. Of the various industrial tomography such as gamma, X-ray, microwave, ultrasonic, optical, electrical resistance tomography (ERT), electrical capacitance tomography (ECT) that are available for process industry applications, ECT is one of the most promising one due to its inherent simplicity, robustness, high speed capability, zero radiation emission, non-invasiveness, non-intrusiveness, low cost and ability to withstand wide range of operational temperatures and pressures [1].

ECT is a tomographic technique that involves the determination of the spatial permittivity distribution of dielectric materials within an object from external capacitance measurement using multiple sensor electrodes mounted on the periphery of the object [2]. The ECT system

typically consists of three units, namely the ECT sensing system, Data Acquisition System (DAS) and the Computing System. The ECT sensing system consists of an object (e.g., a pipe) and sensing electrodes, which are mounted on the object's periphery; this unit is used to obtain measurement values of the dielectric material within the object where they are mounted. Data Acquisition System (DAS) unit is used to acquire data obtained by the sensors and subsequently transfer the data in machine-readable form to the computing system. The computing system consists of a computer built to ECT manufacturer's specification and proprietary software, which comprises algorithms that aids real time and offline data reconstruction, tomographic image display and data analysis.

The ECT system was reportedly used in pipeline flow visualization at the University of Manchester in the early 1990s [3]. The success of earlier studies led to the subsequent use of ECT in visualizing multiphase flows in oil pipelines [1]. Nevertheless, visualization of multiphase flow using ECT techniques were concentrated on low viscous oils (less than 20 cP). Research work using ECT for applications higher than 1000 cP was not found in literature by the authors. Also, in multiphase flows, flow patterns for flows consisting of high-viscous liquids are significantly different from low-viscous liquids. Gokcal *et al.* [4] observed an increase in slug frequency and liquid holdup with a corresponding decrease in slug length as oil viscosity was increasing. Márquez and Trujillo [5] affirmed the difference in flow pattern at increased liquid viscosity when they noted in their work that slug region increased with increase in liquid viscosity. This study was concerned with high-viscous oil applications due to its increasing importance as a veritable energy source. Factors such as depleting conventional oil reserves, increase in world energy demand, technological advances (in heavy oil production), availability of huge heavy oil reserves and prevailing oil prices have combined to make heavy oil one of the leading sources of energy. Previous studies of ECT on multiphase applications are outlined below.

Gamio *et al.* [6] used an ECT system they designed to visualize two-phase flow consisting of oil and gas in a 7.62 cm pressurised test loop. Nitrogen gas and Exxsol D80 oil were respectively used as the gas and oil phases in the study. Different flow patterns were obtained though variations in the flow rates of oil and gas. Tomographic images were obtained for each flow condition and the results obtained were validated with video graphic images obtained through a transparent section in the flow loop as well as with the flow pattern map. Their work was based on oil with viscosity of 1.7 cP at 25 °C, and the study did not involve flow measurement such as liquid holdup.

Zhang and Wang [7] used a twin-plane dual modality (ECT/ERT) system developed by Tianjin University for the identification of oil-gas two-phase flow patterns. Only the ECT sensor outputs were used and the ECT sensor consisted of 12 electrodes mounted at the circumference of the pipe. A 0.6 m long horizontal test section with pipe internal diameter of 80 mm was used for the study. Nylon plastic pellets were used to stimulate each flow pattern. In the work, ECT identification of stratified flow, annular flow, core flow and full pipe flow patterns agreed with the Support Vector Machine (SVM), which is a technique based on statistical theory. However, this study reported very limited experimental data. The test was done under static conditions and the authors did not list the properties of the fluids used.

Baker *et al.* [8] used ECT to visualize the time varying cross sectional distribution transients in two-phase gas-liquid stratified/slug flow. The experiments were conducted in a 16.7 m long pipe with internal diameter of 0.038 m. Air and kerosene (viscosity of 3 cP at 25 °C) were used as the gas and liquid phase respectively. The maximum gas superficial velocity used was 12 m/s while the superficial velocity of the liquid was 0.5 m/s. An 8 electrode ECT sensor was used to visualize the cross sectional distribution of the phases in flow. Stratified and slug flows were clearly shown in the tomographic images obtained for both the high and low liquid superficial velocities. However, ECT images and visual observations via the transparent pipe section indicated either slug or stratified flows in disparity to annular flow predicted by the flow pattern map of [9]. Void fractions data obtained from ECT were found to be in agreement with those obtained from other studies in literature with similar fluid properties.

Isaksent *et al.* [10] used capacitance based tomography system for interface measurement in separation vessels. An eight-electrode capacitance sensor mounted circumferentially around a plexi-glass separator with a 60 cm long earthed screen surrounding the electrodes was used. The test fluids used were compressed air, tap and salt water as well as two types of oil (Exxol D80 and D100) with dielectric constant near 2.1. The tomography system was tested for both oil/air separation and oil/water/air separation. The oil/foam/air was conducted by creating enough foam inside the separator by means of high oil and gas flow rates which resulted in severe liquid motion. The tomographic system detected the foam thickness inside the separator above 5 to 10 cm. The reconstructed foam layer thickness was observed to give a good representation of the foam layer thickness inside the separator. The average absolute and maximum absolute errors were 0.3 and 2 cm, respectively. Water-oil-air test was also carried out for water conductivities of  $4 \times 10^{-3}$  S/m and 5 S/m (salt water). The absolute average error for both tap and salt water height and oil thickness were within 0.5 and 1.0 cm respectively.

Warsito and Fan [11] used a capacitance sensor array that comprised a twin plane sensor using 12 electrodes for each plane with each electrode measuring 5 cm in length to identify flow patterns in a gas-liquid two phase flow and a three phase gas-liquid-solid flow in a bubble column. For the gas-liquid fluid, air was used as the gas phase while Norpar 15 (paraffin) and Paratherm heat transfer liquids were used as the liquid phase. Norpar 15 has a density of 773 kg/m<sup>3</sup> and a viscosity of 0.253 mPa·s. Paratherm has a density and a viscosity of 870 kg/m<sup>3</sup> and 0.317 mPa·s respectively. Polystyrene beads with density and diameter of 1020 kg/cm<sup>3</sup> and 2 mm, respectively, were used as the solid phase in the gas-liquid-solid system. The three-phase system was essentially a dielectrically two-phase system, enabling the measurement of the gas holdup alone in the gas-liquid-solid system independent of the other two phases. This is because the polystyrene beads have permittivity similar to that of Paratherm. The data acquisition system captured data at 100 frames per second. Iterative Linear Back Projection (ILBP) algorithm was used for the image reconstruction of the multiphase flow at 32 x 32 pixels per image. The study showed that ECT could be suitably applied in imaging gas-liquid as well as gas-liquid-solid flow systems with the image reconstruction method developed by the authors. It was observed that the technique used had no limitations on the maximum gas holdup but it proved difficult to measure small gas holdup due to the small signal-to-noise ratio.

Jeanmeure *et al.* [12] developed a design that enabled the use of ECT to directly identify flow patterns in a two-phase gas-oil flow. The study involved the flow identification and control in an air-kerosene flow in horizontal piping by using 8-electrodes ECT system and T-junction separator. This was done for a reduced set of interest of flow patterns with distinctive characteristics (annular and stratified flow). The method produced relatively fast images at 200 images per second and was used to detect slug flow to enable actions that will prevent undesirable effects on unit operation equipment downstream. The density and viscosity of the oil used in the test were 973.05 kg/m<sup>3</sup> and 0.026 Pa·s respectively. The flow pattern identification was performed using the visual inspection of the flow in transparent pipe section and quantifying the fluctuations of the void fraction and dynamic pressure from the capacitance reading and pressure readings respectively using Probability Density Function (PDF) and Power Spectral Density (PSD) function of the time trace signal. The study concluded that capacitance sensors were very sensitive to flow regime change and could be used to identify the different flow patterns. This study was, actually, on low viscous oil, and tomographic images were not reported there.

Similarly, gamma radiation methods, being non-intrusive methods, have been frequently used for the measurement of component volume fractions in multiphase flow systems. For most applications, it is the attenuation of radiation (gamma-ray) that serves as the source for the measurements. Gamma densitometry has numerous advantages in terms of its higher penetration capabilities over other radiation attenuation methods (i.e., neutron beams) thereby making it a more ideal system for the measurement of phase fractions in large industrial systems.

From the literature reviewed above, it is obvious that most existing studies were based on low viscous oil, hence, a basis for this study to consider high-viscous flows using ECT. The capability of ECT in high-viscous flows (up to  $\mu=7500$  cP) was thus investigated under static (bench) and dynamic (flowing) conditions. Tomographic images of ECT and temporal variations of liquid holdup measurements through time series plots were used to identify flow patterns. Gamma densitometer (a device for measuring the density of fluids in a completed well, pipeline or process equipment, using a radioactive source of gamma rays and a detector), visual observations and video recordings were used to validate the measurements of the ECT.

## 2. Experimental setup

In this study, two experimental test facilities in the Process and Systems Engineering (PASE) Laboratory were used for the dynamic (flowing) test, and the bench test was also conducted. Actually, 1 and 3-inch multiphase facility are similar in design with both having capabilities to operate under varieties of multiphase flows consisting of gas, water, oil and sand. The 3-inch multiphase facility (Figure 1) that was used in this work is described below.

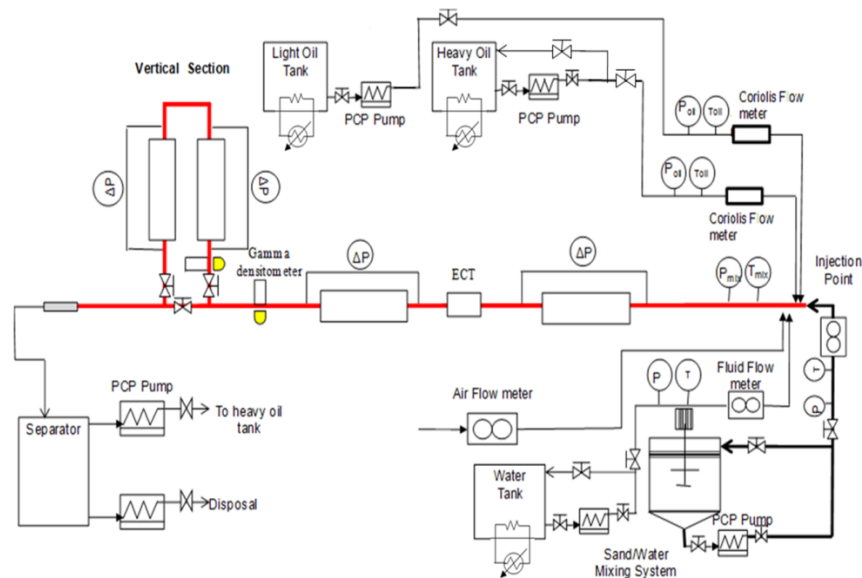


Figure 1. Schematics of the 3-inch multiphase facility at Cranfield University

The 3-inch multiphase facility is similar to the 1-inch facility. It is, actually, a scale up of the 1-inch facility. It is once through and consists of a 0.75 mm ID Perspex pipe with length of about 17 m. It has vertical and horizontal pipe sections, but for purposes of this study, emphasis will be laid on the horizontal section since this was the one used. The observation section of the facility was placed 150 pipe diameters upstream of the last injection point to ensure complete flow development in the horizontal section. Free air was received and compressed by an AtlasCopco® Screw Compressor with maximum discharge pressure and capacity of 10 barg and  $400 \text{ m}^3 \cdot \text{hr}^{-1}$  respectively. Compressed air was discharged to a  $2.5 \text{ m}^3$  air tank before it was delivered to the test section to avoid pulsating supply. At the tank, it was regulated to about 7 barg and fed to the test section where two gas flow meters, a 0.5-inch (Prowirl 72F15 DN15) vortex flow meter with range of  $0\text{-}20 \text{ m}^3/\text{hr}$  and a 1.5-inch (Prowirl 72F40 DN40) vortex flow meter with range from  $0\text{-}130 \text{ m}^3/\text{hr}$ , both manufactured by Endress+Hauser, were used for air metering. Air was fed to the test section through a 2-inch steel pipe in-line with the horizontal test section.

A tank of capacity of  $2 \text{ m}^3$  was used to store heavy-oil from where it was pumped using a variable speed progressive cavity pump with maximum capacity of  $17 \text{ m}^3/\text{hr}$ . Endress+Hauser's Promass 831 DN 80, coriolis flowmeter with range of  $0\text{-}171 \text{ m}^3/\text{hr}$ , was used in oil metering. The flow meter had three outputs: mass flow rate, density and viscosity.

A refrigerated bath circulator manufactured by Thermal Fisher was used for temperature control. Coils which were connected to the circulator were submerged in the oil tank, and hot or cold glycol was passed through the coils to regulate the oil temperature and, hence, its viscosity. The circulator temperature ranged from 0 to 50°C with an accuracy of  $\pm 0.01^\circ\text{C}$ . Data were acquired from the facility as raw voltage (0 – 10 V) using the data acquisition system, NI USB-6210, and they were converted to engineering units using Labview® version 8.6.1. The 3-inch ECT sensor was installed just after the viewing sections, which was about 155 pipe diameters downstream of the feeding point for oil and gas. The slurry and water systems are not described even though they are shown in the test facility schematics because they were not used in this study.

CYL 680, a mineral oil manufactured by Total® with density of  $920 \text{ kg m}^{-3}$  and viscosity of 3000 cP at 20 °C was used as the liquid phase (heavy-oil) in the dynamic test. CYL 680 and EDM 250, which is a dielectric oil type manufactured by Rustlick™ with viscosity 4 cP at 20 °C and density of  $801 \text{ kg m}^{-3}$ , were used in the bench test. For both tests, the gas used was atmospheric air, and it was compressed in the case of the dynamic test.

The ECT device used in this study was manufactured by Industrial Tomography Systems (ITS) in Manchester, United Kingdom. The system is made up of a sensing unit, data acquisition and a computing system. The sensing unit consists of a flexible copper laminate engraved with a predetermined electrode pattern and placed around steel pipe circumference with internal diameters of 1 and 3 inch respectively. Computer system and data acquisition software makes up the computing system. The software, Multi Modal Tomography Console (MMTC) has a VC++ Graphical User Interface (GUI), which was used to view the process of interest online and for tomography data management. Collated data could be viewed offline using another ITS proprietary software, Toolsuite V7. The Linear Back Projection (LBP) algorithm was used for image reconstruction in both software.

Furthermore, a gamma densitometer was used for phase fraction measurement. A fixed single-beam gamma densitometer manufactured by Neftemer Limited made up of a gamma source block and a Sodium Iodide (NaI) scintillation radiation detector was installed on the 3-inch facility. A 5.5 GBq Caesium-137 radioisotope was contained in the gamma radiation source block enclosed within a lead radiation protection shield protected by stainless steel. The radioisotope in the gamma densitometer was a dual-energy source emitting gamma rays in two broad photon energy levels. The 662-keV high-energy level was sourced from the gamma radiation transmission while the lower energy level range of 100 keV–300 keV was sourced from the scattered gamma radiation. Sodium iodide (NaI) scintillation radiation detector was used for the measurement of two separate sets of gamma attenuation data for the high and low energy levels with a sampling rate of 250 Hz. A detailed description of the gamma densitometer (see pictorial view in Figure 2) used for this investigation has been presented by [13].

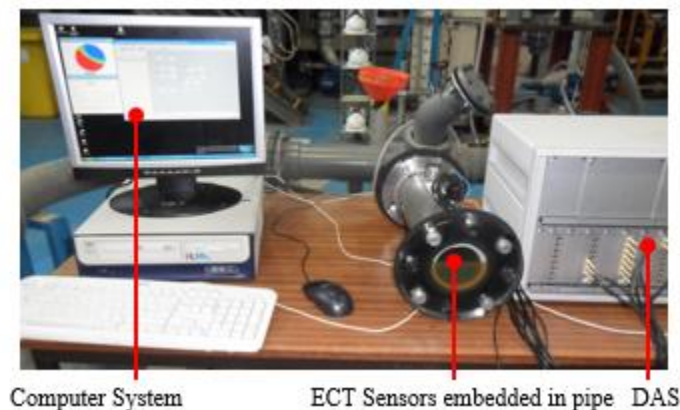


Figure 2. ECT static (bench) test experimental setup

In this study, the static (bench) and dynamic (flowing) test were conducted in the 1 and 3-inch facility using two ECT sensors of the same (test facility) size. In the static test, dielectric oil (4 cP at 25°C) and CYL 680 oil (3,000 cP at 25°C) were used with air as the gas phase. Liquid holdup measurements, tomographic images and raw capacitance signals were obtained from ECT for both sensors. The sensors were first calibrated by taking the capacitance readings for completely empty ECT sensor (full air) and recorded as the low reference since it is the low permittivity medium; the sensor was then filled with oil and recorded again to obtain the high reference since it was the high permittivity medium. The calibrated results were used as references for both the static and dynamic test. In the static test, emphasis was laid on the ability of the ECT to predict the liquid holdup measurement, visualize tomographic images and the raw capacitance measurement. In the ECT system, tomographic images were obtained essentially from the reconstruction of the raw capacitance data obtained by the sensors during sensing to pixel permittivity using some form of algorithm (in this case, the Linear Back Projection, LBP). In LBP, reconstruction was done in the Multi Modal Tomography Console (MMTC) software. A grey level was assigned to each of the 66 sensing areas. By superimposing the grey levels on the areas, the region where the object to be visualized was located became enhanced. 66 element vector with each value set as 1 for object presence and 0 for none presence was used to relate the 66 sensing areas. By multiplying the corresponding segment vector,  $V$ , with the 66-capacitance measurement values ( $m_1, m_2, \dots, m_n$ ), the grey level,  $G$  was obtained. For a  $K$  number of segments, Equation (1) [14] was thus obtained.

$$\begin{pmatrix} G_1 \\ G_2 \\ \vdots \\ G_{K-1} \\ G_K \end{pmatrix} = \begin{pmatrix} V_1 \\ V_2 \\ \vdots \\ V_{K-1} \\ V_K \end{pmatrix} \begin{pmatrix} m_1 \\ m_2 \\ \vdots \\ m_{K-1} \\ m_K \end{pmatrix} \quad (1)$$

The equation thereby reduced to a matrix multiplication problem.

### 2.1. ECT referencing

Representative tomographic images results obtained in the 3-inch sensor for the air-oil system in both the heavy-oil and air are shown in Figure 3. The images show the first tomogram which is completely blue in colour indicating a completely empty sensor (100% air), that is, 0% liquid holdup to a completely filled sensor as shown in the last tomogram, and a total red colour indicating 100% liquid holdup (completely filled with oil). The two tomograms mentioned were subsequently used as the references.

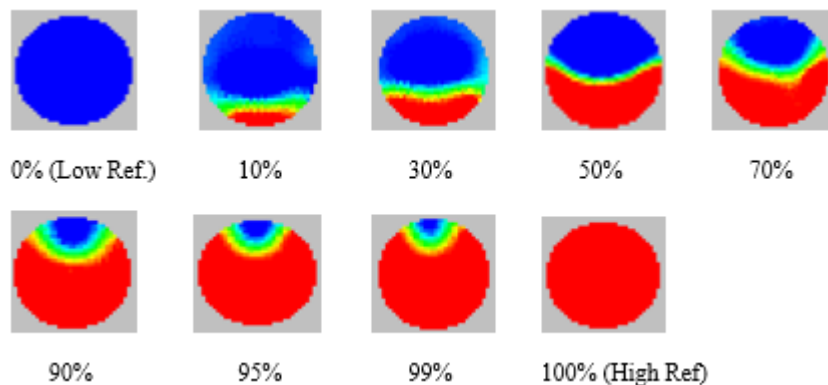


Figure 3. Tomographic images of different liquid holdup (%) for dielectric oil (viscosity: 3000 cP; ECT sensor: 3 Inch)

The tomographic images clearly indicated an increase in the red section (oil content) as the sensor was filled with oil during the bench test. The interface between the oil and air in the tomograms were indicated by a yellowish green colour; this region is normally considered as aerated oil. The tomographic images showed no noticeable effect of viscosity and pipe diameter difference on the ECT sensor. The test was conducted for both 4 cP (dielectric) and 3000 cP (CYL 680) oil with air as the gas phase using both the 1 and 3-inch sensors, and similar results were observed for all four cases studied.

It is worth noting that even though ECT displayed the tomographic images as a “representative” of the holdup value, the actual liquid holdup was obtained using the Maxwell’s expression (ITS, 2000) given in Equation (2).

$$\alpha = \frac{2\sigma + \sigma_2 - 2\sigma_{mp} - \frac{\sigma_{mp}\sigma_2}{\sigma_1}}{\sigma_{mp} - \frac{\sigma_2}{\sigma_1}\sigma_{mp} + 2(\sigma_1 - \sigma_2)} \quad (2)$$

In the equation above,  $\alpha$  is the volume fraction of the dispersed material,  $\sigma_1$ ,  $\sigma_2$  and  $\sigma_{mp}$  are the permittivity of the continuous phase, that of the dispersed phase and the reconstructed measured permittivity respectively.

### 3. Results and discussion

Results obtained from experimental investigations carried out in this study are presented in this section. Liquid holdup plots obtained in the study are shown in Figure 4 and 5. The solid line indicates an ideal case in which the measured and actual liquid holdup values are equal while the dotted line indicates the error margin from the ideal case. Liquid holdup measurement for 1 and 3-inch sensor at 3000 cP oil viscosity are shown in Figure 4. For both sensors, similar results were obtained and the effect of increase in size from a 1 to 3-inch sensor was not significant. About  $\pm 10\%$  error margin was observed for both sensors thus showing no significant effect of increase in pipe diameter on ECT performance. ECT performance was also evaluated for the 4 cP oil under static condition; the results obtained were compared with the liquid holdup measurements for 3000 cP oil and they showed no significant effect as a result of the change in viscosity. The curved interface in the tomograms are related to the LBP algorithm used in image reconstruction.

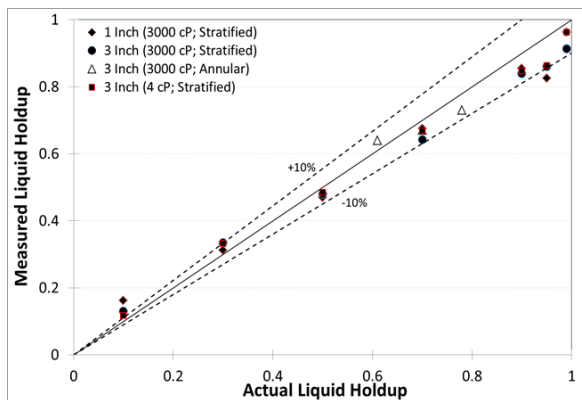


Figure 4. Liquid holdup comparison for 1 and 3-inch sensor ( $\mu = 3000$  cP) oil

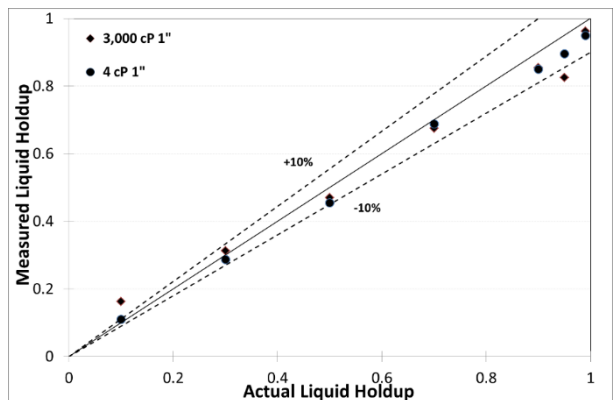


Figure 5. Viscosity comparison for 1-inch sensor

From Figures 4 and 5, it was observed that ECT could be used to predict the liquid holdup for actual liquid holdup values from 50% and above while overestimating liquid holdup values below 50%. In this case, the error margin was relatively lower at the lower liquid holdup values. This trend was observed for both 1 and 3-inch sensors as well as the two viscosities tested. Error margins at the liquid holdup values close to the high reference (full pipe) was seen to improve relatively to that in the mid liquid holdup values. This phenomenon is attributed to the LBP algorithm used in the image reconstruction and the fact that the sensor was

calibrated at the two terminals, the low and high reference; hence, relatively similar trends were noticed in literature for other sensing instrument such as gamma [15].

### 3.1. Flow pattern identification with ECT

Annular flow pattern was modelled on the bench (static) by inserting polyvinyl chloride (PVC) pipes of cylindrical shape with varying outer diameter (36 – 48 mm) into the oil filled sensor in the vertical position. The low reference used here was the PVC pipe inserted into the empty sensor while the high reference was oil. Figure 6 shows that for annular flow, the error margin ( $\pm 5\%$ ) is well within that of the stratified static test, possible reasons for error difference were the sensor positioning and pipe material used.

Air-oil dynamic tests were conducted in the 1 and 3-inch multiphase facilities for viscosities of 1000, 3000 and 6000 cP. ECT was used to identify flow patterns and validated by visual observations in the sections that follow. Superficial gas and liquid velocities used in the study were 0.3 – 9 m/s and 0.06 – 0.1 m/s, respectively.

Some representative stacked tomographic images (time series of tomographic images taken from frames in consecutive sequence) for the 3-inch rig at 1000 cP, with  $V_{sg}$  values ranging from 0.3 – 9.0 m/s and a  $V_{so}$  value of 0.1 m/s are shown in Table 1. The images obtained provided information on the phase distribution in the pipeline during each flow condition. For  $V_{so}$  value of 0.1 and  $V_{sg}$  value of 0.3 – 0.5 m/s at 1000 cP, plug flow regime was observed. This flow pattern consisted of two characteristic tomographic images: one in which the tomogram showed a stratified layer of red at the bottom (indicating oil) with blue (gas) at the top section of the pipe. At certain intervals, this image almost changed completely to red (oil), and this period indicated the passage of the entire oil with negligible amount of gas, hence the plug body. In the stack images shown in Table 1, it is seen that oil (red colour) completely bridged to the top as the plug body was passing. This flow pattern was classified as plug flow based on the definition of [16], which states that plug flow is a limited case of slug but with the liquid plug being free of entrained gas bubbles. The yellowish-green and red colours observed at the pipe wall (in the stacked images) can be explained by the oil film coating on the walls of the pipe housing the sensor as a result of the high-viscous property of the oil.



Figure 6. Film and plug unit at  $V_{so}=0.1$  m/s and  $V_{sg}=0.3$  m/s,  $\mu_l = 1000$  cP

A plot of the concentration (liquid holdup) time series was also analysed for flow patterns observed in the conditions stated above, and the plot showed intermittent behaviour, fluctuating from a low concentration of about 0.65 to as high as 1 in some cases. Plug/slug body were defined as such when the liquid holdup rose above 0.75 m/s. The low concentration value indicated the film region. Here, the combine flow of air and oil ensured that the liquid holdup value was relatively lower while the high concentration value indicated the passage of the plug body where very little air was contained in the flow and the liquid almost completely occupied the pipeline. The Probability Mass Function plot further confirmed the flow pattern obtained at the aforementioned flow conditions, which clearly showed a bi-modal distribution. ECT measurement was validated by a video recording, which was showing the plug flow pattern observed through physical inspection and recordings. Flow patterns observed at  $V_{so}$  value of 0.1 m/s and  $V_{sg}$  value of 0.3 -0.5 m/s at 1000 cP was found to be, actually, plug flow. It had two characteristic units that flowed intermittently. A film unit in which the less dense gas flowed on top of the denser liquid in a stratified pattern. This unit was disrupted at

certain intervals by long plug bodies flowing through. The plug was observed to cover the entire viewing section with no visible gas entrainment as shown in Table 1.

For  $V_{so}$  value of 0.1 and  $V_{sg}$  value of 0.7 – 2.0 m/s at 1000 cP, slug flow regime was observed. The tomographic images obtained were similar to those in plug flows differing only in the appearance of blue colour during intervals where the tomograms changed from stratified blue (at the top) and red (at the bottom) to a wholly red colour with little quantity of blue as presented in Figure 7.

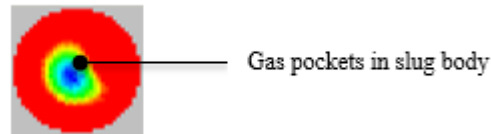


Figure 7. Tomogram showing gas entrained in liquid slug unit at  $V_{so}=0.1$  m/s and  $V_{sg}=1.0$  m/s with oil viscosity of 1000 cP

In the tomographic stack images in which the complete red image earlier seen in plug flow was not present, a dominant red colour was observed but with visible blue albeit small in size. This was attributed to the presence of entrained gas bubbles as the slug body passes. The slug body was shorter and more frequent as indicated in the stacked images at these flow conditions. The concentration time series plots and PMFs, however, did not show any significant difference between slug and plug flows. Based on the definition of Barnea *et al.* [16] this flow pattern was called slug flow. Video recordings showed a similar behaviour with plug flow differing in the slug body being shorter, more frequent and more energetic relative to the plug body. Gas bubbles were also observed in the slug unit as well as increased instability of the film region. The film region instability, change in slug length and increase in flow intensity were due to the increased kinetic energy of flow as a result of the increase in gas superficial velocity.

At  $V_{sg}$  values of 3 m/s in the 1000 cP test, flow regime observed in the stack images was a transition between the slug and wavy annular flow. The oil was seen to have insufficient energy to bridge the gas core thus forming a kind of wavy pattern around the gas as shown in Figure 8. This classification was chiefly subjective, but the PMF plot laid further credence to this as the hitherto, bimodal distribution in plug and slug flows merges partially with each other. This regime was defined as blow-through-slug or pseudo-slug based on the definition of Wong and Yau [17]. In the video recordings, a further increase in  $V_{sg}$  caused the gas kinetic energy to acquire even more momentum resulting in slugs requiring relatively larger energy to bridge the liquid film. It is similar to the wavy annular flow differing only in the fact that the gas velocity is not high enough to sweep the liquid to the top of the pipe.

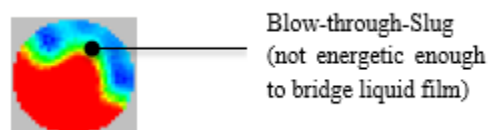


Figure 8. Tomogram showing Pseudo-Slug body at  $V_{so}=0.1$  m/s and  $V_{sg}=3.0$  m/s for oil viscosity of 1000 cP

Finally, at  $V_{sg}$  value of 7 – 9 m/s with oil viscosity of 1000 cP and 5 – 9 m/s, the stack tomographic images showed a wavy flow structure between the gas-oil interface, and the tomograms were similar to the pseudo-slug flow patterns but with relatively low penetration height into the gas zone. The concentration time series also showed a high fluctuation in behaviour with the PMF showing unimodal distribution. In the video recordings, the increased  $V_{sg}$  value caused increase in dissipated energy along the flow resulting in large amplitude of waves at the oil-gas interface. The top of the pipe wall was significantly wetted by oil with gas continually sweeping liquid at the interface to the top of the pipe. Most of the oil in flow, however, remained at the bottom of the pipe (due to gravity) with gas predominantly flowing at the centre and thin oil film at the top. The PMF, liquid holdup plot and the tomographic

images obtained from ECT showed promising results in the capability of ECT to visualize high-viscous oil and gas flows as validated by the video recordings obtained during the study.

Flow pattern maps from the study are shown in Figure 9 and 10. From the figures, an increase in viscosity was seen to result in a corresponding increase in the slug/plug flow pattern region. This was found to agree with the conclusion drawn by Márquez and Trujillo [4] and Gokcal *et al.* [4]. Also, an increase in the oil velocity had similar effects on the flow pattern within the range of superficial oil and gas velocities tested.

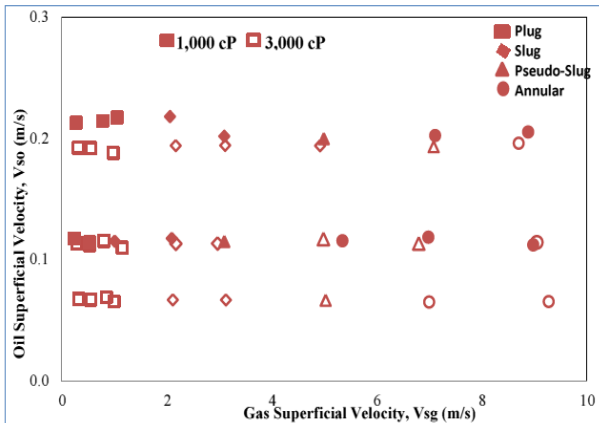


Figure 9. Flow pattern map for 1-inch multiphase facility

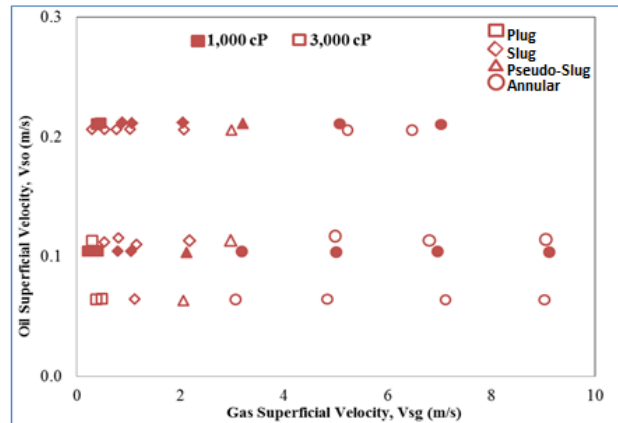


Figure 10. Flow pattern map for 3-inch multiphase facility

### 3.2. Validation of flow patterns obtained by ECT with gamma densitometer

A representative time series and PDF plots of the time varying liquid holdup measurement of ECT and Gamma densitometer measurements are presented in Table 2. Both data obtained from the 3-in pipe ID horizontal test facility are shown for 20 s each to facilitate a clear representation of the results.

At gas superficial velocity of 0.3 m/s, the ECT time series plots showed fluctuations in waveforms. This was an indication of the plug flow pattern in this flow condition. The crests of the waveforms indicated elongated liquid body passage, and each crest was observed to be a result of the sudden increase in the liquid holdup as the liquid bridged the entire pipe cross section. The troughs, which were indications of the film region passage, were characterized by relatively low liquid holdup values, which were explained by the increased void fraction as the liquid bridge hitherto prevalent in the elongated liquid body exited the observation section. Similar waveform characteristics were observed in the Gamma waveform signals shown in Table 2. PDF plots for this flow condition showed a bimodal distribution having two characteristic peaks with one at the higher holdup value indicating the slug liquid body while the other was representing the slug film.

At Vsg of 3.0 m/s, the flow pattern entered its transition region (pseudo-slug), and it was observed that both the ECT and gamma time series plots indicated less frequent crests, which was a result of the reduced intermittency in the flow. PDF plots from both ECT and Gamma indicated different modal distributions. This is as a result of the increased transient nature of the transition flow pattern and/or limitations of the single beam Gamma device used in this case, which was impeding its ability to capture clearly the features of the transition region.

For Vsg values of 9 m/s, both Gamma and ECT time series analysis shows a chaotic behaviour in the time series waveforms with no distinguishable crest or trough. The PDF, at this flow condition, showed a unimodal distribution which clearly suggested the non-intermittency of the flow pattern.

It can therefore be inferred that within the experimental test matrix and test conditions of this study, flow patterns identified by ECT were similar to those identified by Gamma densitometer.

Table 1. ECT results for oil viscosity 1000 cP oil superficial velocity 0.1 m/s with different gas superficial velocities (3-inch ECT sensor)

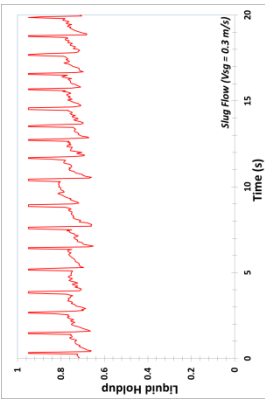
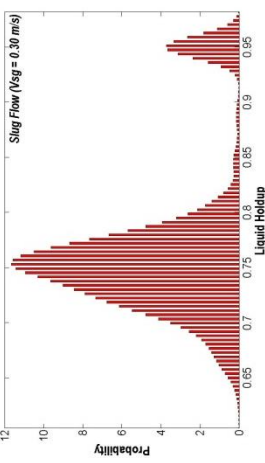
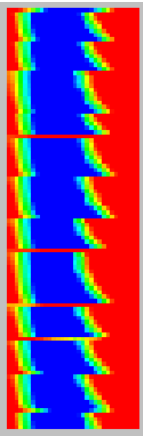
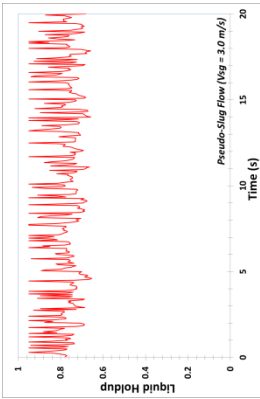
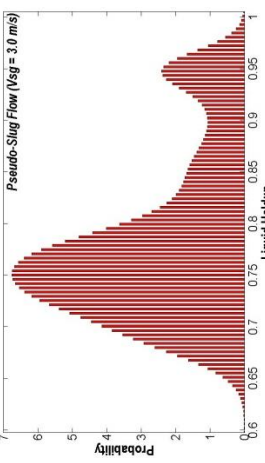
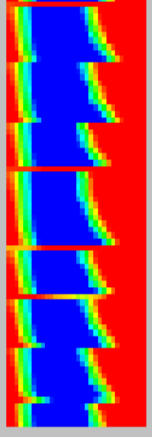
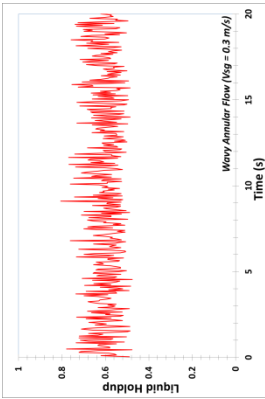
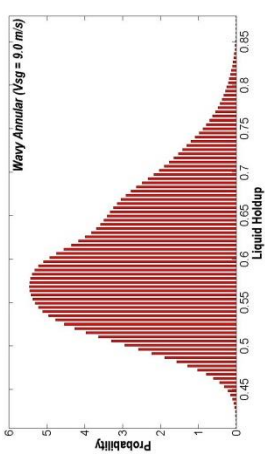
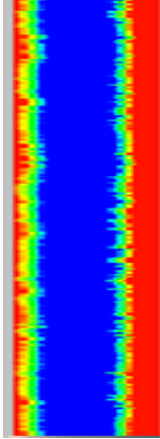
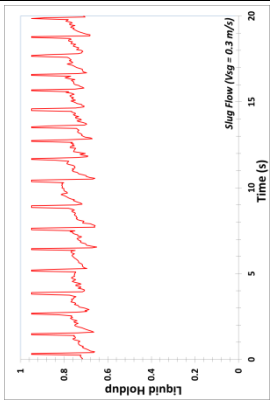
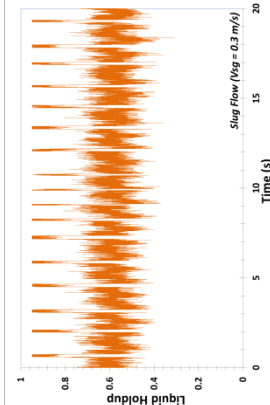
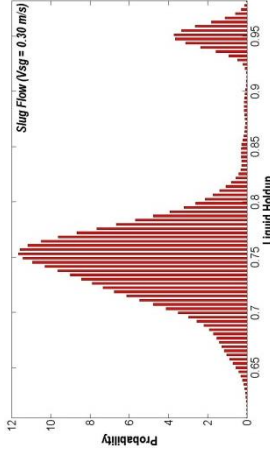
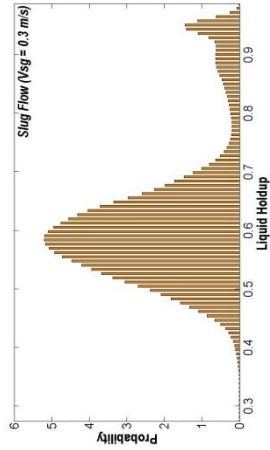
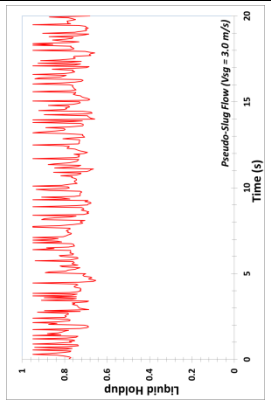
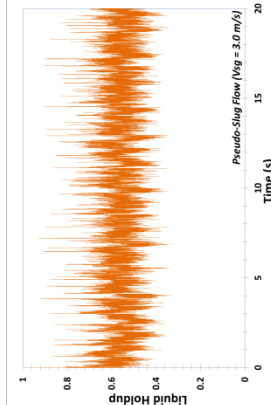
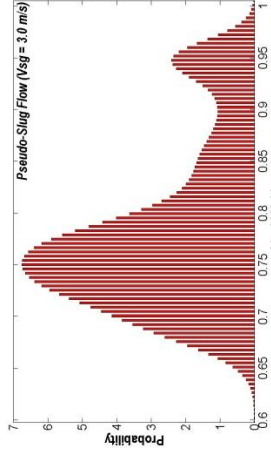
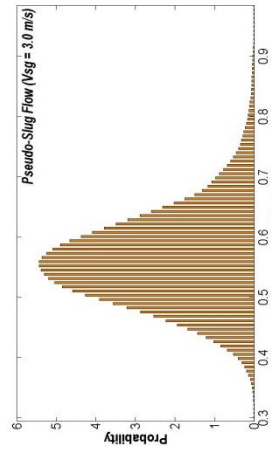
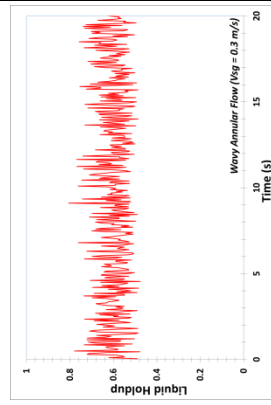
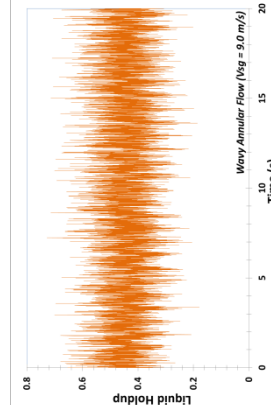
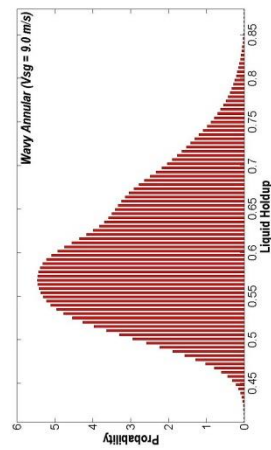
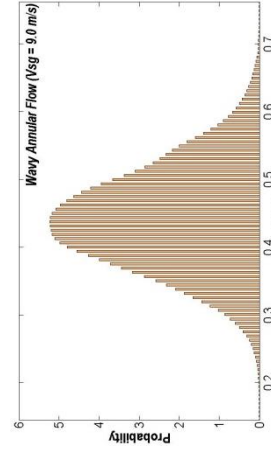
V <sub>sg</sub>	ECT Time Series Plots	ECT PDF Plots	Stacked Images	Stacked Images
0.3 m/s	 <p>Slug Flow (V<sub>sg</sub> = 0.3 m/s)</p>	 <p>Slug Flow (V<sub>sg</sub> = 0.30 m/s)</p>	 <p>Plug Flow</p>	 <p>Plug Body Film Region</p>
3.0 m/s	 <p>Pseudo-Slug Flow (V<sub>sg</sub> = 3.0 m/s)</p>	 <p>Pseudo-Slug Flow (V<sub>sg</sub> = 3.0 m/s)</p>	 <p>Pseudo-Slug</p>	 <p>Pseudo-Slug Flow</p>
9.0 m/s	 <p>Wavy Annular Flow (V<sub>sg</sub> = 9.0 m/s)</p>	 <p>Wavy Annular (V<sub>sg</sub> = 9.0 m/s)</p>	 <p>Wavy Annular Flow</p>	 <p>Wavy Annular Flow</p>

Table 2. ECT results and Gamma Densitometer validation for oil viscosity 1000 cP oil superficial velocity 0.1 m/s with different gas superficial velocities (3-inch ECT sensor)

Vsg	ECT Time Series Plots	Gamma Time Series Plots	ECT PDF Plots	Gamma PDF Plots
0.3 m/s				
3.0 m/s				
9.0 m/s				

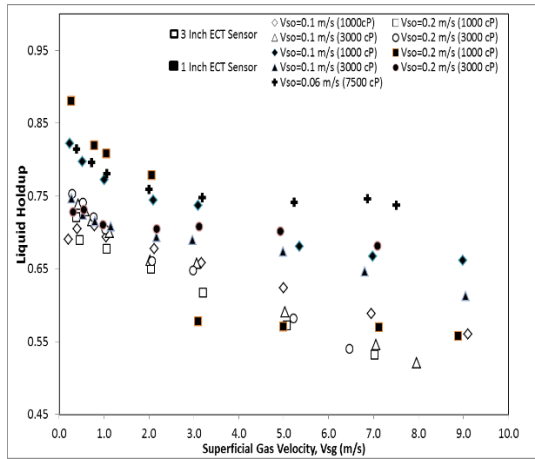


Figure 11. Plot of liquid holdup against Vsg at different Vso for 1- and 3-inch ECT sensor

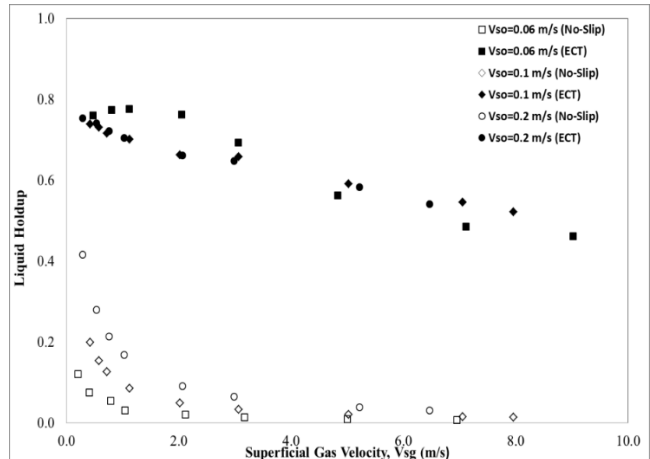


Figure 12. Plot of liquid holdup predicted by "No-Slip" equation and ECT sensor against Vsg (m/s) for the 3-inch test facility at oil viscosity of 3000 cP

Figure shows time averaged liquid holdup measurement obtained for 60 s from ECT in both the 1- and 3-inch test facility for viscosities ranging from 1000 – 7500 cP. The data plot showed a general trend of reduction in liquid holdup value as the gas superficial velocity was increasing. This was expected to be so in order to satisfy the continuity equation. As the gas superficial velocity was increased, the gas was observed to occupy more cross sectional area in the pipe resulting in a corresponding reduction of the liquid holdup in the cross sectional area of the pipe. An increase in the viscosity of the oil resulted in an increase in the liquid holdup at fixed Vsg and Vso. This was due to the fact that an increase in viscosity resulted in an increase in the shear stress (resistance to flow) of the oil. A reduction in the amount of entrained gas in the slug body (for slug flows) was also observed visually as well as from the time series trace in ECT. The gas kinetic energy hitherto sufficient to displace a particular amount of oil then became insufficient, thereby resulting in more liquid remaining in flow and thus increased liquid holdup. A comparison of the liquid holdup obtained from ECT to that of the "no slip" liquid holdup as shown in Figure was found to show a similar trend. However, the liquid holdup values were significantly different; this was due to the "no slip" assumptions in addition to the increased liquid viscosity tested.

#### 4. Conclusion

ECT provided good tomographic images and liquid holdup measurements under static (bench) conditions. The results obtained showed that the measurement of ECT was accurate to within  $\pm 10\%$  of the actual liquid holdup under stratified static conditions. Under dynamic (flowing) conditions, ECT was able to provide good tomographic images for the distribution of the phases in flows - plug, slug, pseudo-slug (blow-through-slug) and annular flows - that were observed. PMF plots of the liquid holdup data and the time series were used to further identify the different regimes. Flow patterns obtained were validated with the aid of video recordings and gamma ray densitometer. Liquid viscosity and pipe diameter had no significant effect under static conditions on ECT performance. However, for dynamic tests, increase in liquid viscosity led to a corresponding increase in the oil film coatings on the sensor walls. Shorter slugs and increased slug frequency with increase in liquid viscosity was clearly visualized by ECT. This was found to be in agreement with the studies performed by Márquez and Trujillo [5] and Gokcal et al. [4] for high viscous oil-gas flows.

#### Acknowledgement

The authors acknowledge the contribution of the Laboratory Manager, Technicians, Research Staff Members and Students in the Oil and Gas Engineering Centre of Cranfield University for their help and support rendered in the course of this research work.

## References

- [1] Yang W and Peng L. Image Reconstruction Algorithms for Electrical Capacitance Tomography. *Meas. Sci. Technol.*, 1996; 14(1):
- [2] Dyakowski T. Process tomography applied to multi-phase flow measurement. *Meas. Sci. Technol.*, 1996; 7. 343–353.
- [3] Beck MS, Byars M, Dyakowski T, Waterfall R, He R, Wang SJ, Yang WQ. Principles & Industrial Applications of Electrical Capacitance Tomography. *Meas. Control*, 1997; 30(7): 197–200.
- [4] Gokcal B, Al-Sarkhi A, Sarica C, and Alsafran EM. Prediction of Slug Frequency for High Viscosity Oils in Horizontal Pipes,” in SPE Annual Technical Conference and Exhibition, 2009.
- [5] Márquez J and Trujillo J. Overview: Slug-Flow Characterization for Heavy-Oil Fields. in *Proceeding of SPE Latin American and Caribbean Petroleum Engineering Conference*, 2010, no. December, pp. 1–3.
- [6] Gamio J, Castro J, Rivera L, Alamilla J, Garcia-Nocetti F, and Aguilar L. Visualization of Gas-Oil Two-Phase Flows in Pressurized Pipes Using Electrical Capacitance Tomography. *Flow Meas. Instrum.*, 2005; 16: 129–131.
- [7] Zhang L and Wang H. Identification of oil-gas two-phase flow pattern based on SVM and electrical capacitance tomography technique. *Flow Meas. Instrum.*, 2010; 21(1): 20–24.
- [8] Baker G, Azzopardi B, and Clark W. Transients in stratified/slug flow – observations using electrical capacitance tomography. in *International Conference on Multiphase Technology*, 2003.
- [9] Taitel Y and Dukler AE. A model for predicting flow regime transitions in horizontal and near horizontal gas-liquid flow. *AIChE J.*, 1976; 22(1): 47–55.
- [10] Isaksent O, Dicot A, and Hammer EA. A Capacitance-Based Tomography System for Interface Measurement in Separation Vessels. *Meas. Sci. Tech*, 1994; 5: 1262–1271.
- [11] Warsito W and Fan L. Flow Structures in Gas-Liquid & Gas-Liquid-Solid Flow Systems Using Electrical Capacitance Tomography. *Chem. Eng. Sci.*, 2001; 56: 5871-5891.
- [12] Jeanmeure L, Dyakowski T, William B, and Zimmerman W. Direct Flow-Pattern Identification Using Electrical Capacitance Tomography. *Exp. Therm. Fluid Sci.*, 2002; 26: 763–777.
- [13] Archibong A, Zhao Y, and Yeung H. Comparison of electrical capacitance tomography & gamma densitometer measurement in viscous oil-gas flows. *AIP Conf. Proc.*, 2014; 1592(1).
- [14] Plaskowski A, Beck MS, Thorn R, and Dyakowski T. *Imaging industrial flows: Application of electrical process tomography*. Bristol and Philadelphia: Institute of Physics Publishing, 1995.
- [15] Åbro E and Johansen G. Improved void fraction determination by means of multibeam gamma-ray attenuation measurements *Flow Meas. Instrum.*, 1999; 10(2): 99–108.
- [16] Barnea D, Shoham O, Taitel Y and Dukler AE. Flow pattern transition for gas-liquid flow in horizontal and inclined pipes. Comparison of experimental data with theory. *Int. J. Multiph. Flow*, 1980; 6(1976): 217–225.
- [17] Wong T and Yau Y. Flow Patterns in Two-Phase Air-Water Flow. *Int. Commun. Heat Mass Transf.*, 1997; 24(1): 111–118.

*To whom correspondence should be addressed: Yahaya D. Baba, Department of Chemical and Petroleum Engineering, Afe Babalola University, Ado-Ekiti, Nigeria, [y.baba9550@gmail.com](mailto:y.baba9550@gmail.com)*